Modeling molecular order and dynamics of a liquid crystal by deuteron NMR

Ronald Y. Dong,[1,2] X. Shen,[2] and G. M. Richards[1]
[1]*Department of Physics and Astronomy, Brandon University, Brandon, Manitoba, Canada R7A 6A9*
[2]*Physics Department, The University of Manitoba, Winnipeg, Manitoba, Canada R3T 2N2*
(Received 17 January 1995)

The quadrupolar splittings in deuterated 4-*n*-hexyloxy-4′-cyanobiphenyl (6OCB) have recently been reassigned with some certainty. This has necessitated a re-evaluation of the fitting of these splittings with the molecular mean field theory. The corresponding spectral densities of motion in this compound could not be successfully modeled before, partly because of the incorrect peak assignments to carbon positions 3 and 4 in the hexyl chain. This difficulty caused us to remeasure these spectral densities as a function of temperature with an improved signal to noise ratio at 15.1 and 46 MHz. In modeling the NMR observables, we found that the presence of an oxygen atom at the top of the hexyl chain has changed the molecular geometry and local energies in the hexyl chain of 6OCB. The observed static and dynamic NMR properties depend on all configurations which are generated using a realistic geometry for the molecule and the rotational isomeric state model of Flory. The additive potential method is employed to construct the potential of mean torque in the nematic phase, which allows the quadrupolar splittings to be calculated. The decoupled model is employed to describe correlated internal modes of motion by means of a master rate equation. Nordio's model of rotational diffusion is used to describe the overall molecular reorientation. Our relaxation data support the recent peak assignments [Liq. Cryst. **17**, 303 (1994)] for deuterated 6OCB. Furthermore, we were able to explain the quadrupolar splittings and spectral densities at various carbon sites of 6OCB in a self-consistent manner.

PACS number(s): 61.30.−v, 33.25.+k

I. INTRODUCTION

Both deuterium and carbon-13 NMR spectroscopy can yield [1] well resolved resonant lines that correspond to various atomic sites in liquid crystals. By means of multipulse NMR techniques, two different deuteron spin-lattice relaxation times can be simultaneously determined to yield individual spectral densities of motion at different sites of a molecule. Ideally, this requires selective deuteration of carbon sites in the molecule and is usually time consuming and expensive. However, many workers [2–6] have chosen deuteron to probe static and dynamic properties of liquid crystal systems. Beckmann *et al.* [2] were the first to propose a model of superimposed rotations to describe fluctuation in orientations of the C—D bonds due to overall and internal motions, and deuteron spin relaxation rates in a partially deuterated 4-*n*-pentyl-4′-cyanobiphenyl (5CB) sample. The molecular core of 5CB is assumed to be relatively massive such that its internal bond rotations in the chain can be treated independently of the overall motion of the whole molecule. Because of its thermal stability and its relatively simple molecular structure, the 5CB molecule has received, both theoretically [7–9] and experimentally [2,10,11], much NMR attention. In particular, correlated internal modes of motion in 5CB were treated by us [7] and by Ferrarini, Moro, and Nordio [8] using a master equation. This approach was necessary, since the quadrupolar splittings of the various deuterons in 5CB could only be modeled [12,13] using all possible configurations generated by the rotational isomeric state (RIS) model of Flory [14].

The RIS model had previously been extended to the time domain [15] to describe correlated internal motion of macromolecules dissolved in solutions. A master equation is constructed to describe transitions among all possible configurations in the pentyl chain of 5CB. The model of Ferrarini, Moro, and Nordio [8] is inherently complex because their master equation includes configuration-dependent frictional effects. The computational effort is extremely demanding because of a large dimensionality in the matrix representation. Our master equation follows the one used for macromolecules in solution, in which three phenomenological rate constants [15] are used to describe elementary jump modes within the chain: one-bond (k_1), two-bond (k_2), and three-bond (k_3) motions. A one-bond rotation involves rotation of the last carbon-carbon bond [i.e., C_5—C_6 in Fig. 1(a)] in the chain, while a two-bond rotation is defined as the rotation of the penultimate bond (i.e., C_4—C_5) in the chain, with all other bonds in the chain remaining the same except the last bond, which may or may not rotate. A three-bond rotation is the interchanging of two alternate bonds, which gives rise to the well known crankshaft motion in the chain. These fast bond rotations are possible because they will not cause a drastic change in the shape of the transformed conformer, thereby minimizing frictional effects with its neighbors. The dimensionality of the transition rate matrix in our master equation is [7,10] much smaller. Despite using phenomenological constants to mimic internal chain dynamics, the model is useful because of its simple computational effort. It is noted that we have used a decoupled model in which the overall motion of a molecule is approximated by a single average rotational diffusion tensor. Coupling between conforma-

tional changes and overall motion of the molecule has been considered [8,9] and may be essential in some cases. Both the small step rotational diffusion model [16] of Nordio and co-workers and the "third rate" model of Vold and Vold [17] may be used to describe overall motions in liquid crystals. The former model describes reorientation of a symmetric top with its rotational diffusion tensor diagonal in a molecule-fixed frame. Freed and co-workers [18] have proposed an anisotropic viscosity model to identify anisotropic properties of mesophases by diagonalizing the rotational diffusion tensor in the director (laboratory) frame. The third rate model is a simple extension of the anisotropic viscosity model achieved by superimposing fast rotations about the long molecular axis on the overall motion of a symmetric top. Since the small step rotational diffusion model has been widely tested by other experimental techniques, it is adopted in the present study of 4-*n*-hexyloxy-4′-cyanobiphenyl (6OCB).

With modern workstations, molecular dynamics (MD) calculations have become feasible [19] in modeling liquid crystal systems with realistic atom-atom potential functions. By parametrizing molecular mechanics force fields, computer simulation of real mesogens is powerful not only in predicting formation of various mesophases, but also in taking the internal structure of a mesogen into account. There are several reports [20–22] on MD simulation of 5CB using atom-atom potentials. Other MD simulation studies include a brief report on 5OCB [23] and those on 4-trans-(4-trans-*n*-pentylcyclohexyl)cyclohexylcarbonitrile (CCH5) [24]. In the work of Komolkin, Laaksonen, and Maliniak [21], it was demonstrated that MD calculations allow an analysis of the trajectories to give NMR related static and dynamic parameters, thereby providing another means of investigating molecular conformations and dynamical variables in liquid crystal systems. In particular, they have shown that MD calculations of rotational diffusion constants in 5CB have reproduced those obtained [7,10] by us from analyzing deuterium NMR relaxation data with the decoupled model. The local motion in the pentyl chain was also addressed by them. The ability to extract from MD calculations quantitative information on local motion remains to be seen. In any case, we hope that the present deuteron study of a larger molecule, namely, 4-*n*-hexyloxy-d_{13}-cyanobiphenyl-d_8 (6OCB-d_{21}), will stimulate MD calculations for comparison.

Several investigators have studied static and/or dynamic properties of 6OCB with deuterium [25,26] and carbon-13 [27] NMR. In a perdeuterated sample, the quadrupolar splittings cannot be unambiguously assigned to the deuterons in the alkyl chain. The mean field theories gave [25,28] the best agreement when the splittings were assumed to decrease sequentially along the chain towards the methyl group. However, Poon, Woolridge, and Fung [27] suggested that the assignments of various peaks based on the ^{13}C-H dipolar couplings in 6OCB should be reversed at the carbon positions 3 and 4. In interpreting the spin-lattice relaxation rates of deuterons in perdeuterated 6OCB [26] based on the overall and internal bond rotations, there were discrepancies between experiment and theory at the carbon positions 3 and 4 when the assignments of splittings given by Counsell *et al.* [25] were used. The disagreements in the assignments of the quadrupolar splittings in the deuterated *n*-hexyl chain have recently been resolved [29] by using partially deuterated derivatives in which deuterons are selectively placed on the *n*-hexyl chain. With the new assignments, the present study aims to resolve the incorrect predictions of quadrupolar splittings in 6OCB of the molecular mean field theory. We found that geometrical parameters used before [25,26] at the oxygen site in the *n*-hexyloxy chain were inappropriate. Furthermore, the decoupled model can also predict the spectral densities of motion over the entire nematic range. As in previous studies [2,10,26], the contribution from director fluctuations [30,31] to deuteron spin relaxation in the MHz region is assumed to be small and can be neglected. Because of apparent discrepancies between theoretical and experimental spectral densities at the carbon positions 3 and 4, as well as the peculiar behaviors of spectral densities at the carbon position 1 [26], we have measured these spectral densities with a much better signal to noise ratio. A brief description of the experiment is given in the next section. The theory and details of molecular parameters used to model both the quadrupolar splittings and spectral densities of motion in the nematic phase of 6OCB are outlined in Sec. III. Section IV gives results and discussion, and Sec. V contains a brief summary.

II. EXPERIMENT

The 6OCB-d_{21} sample was purchased from Merck, Sharp and Dohme Canada and used without further purification. It has a clearing temperature (T_c) of 75 °C. A home-built superheterodyne coherent pulse spectrometer was operated at 15.1 MHz using a Varian 15 in electromagnet and at 46.05 MHz using a 7.1 Tesla Oxford superconducting magnet. The sample was placed in a NMR probe whose temperature was regulated by an air flow with a Bruker BST-1000 temperature controller or by an external oil bath circulator. The temperature gradient across the sample was estimated to be better than 0.3 °C. The $\pi/2$ pulse width of about 3.5 μs was produced by a ENI model LPI10H linear power amplifier. Pulse control and signal collection were done by a General Electric 1280 computer. Following procedures similar to those described elsewhere [32], data reductions, including fast Fourier transform, to obtain partially relaxed spectra were carried out on a PC using Spectral Cal (Galactics Industries), while linear regressions and peak deconvolution to find the Zeeman (T_{1Z}) and quadrupolar (T_{1Q}) spin-lattice relaxation times were performed using Origin (MicroCal). A broadband Jeener-Broekaert (JB) sequence (Fig. 1) with the appropriate phase cycling of radiofrequency and receiver phases [31] was used to simultaneously measure T_{1Q} and T_{1Z}. Despite the broadband excitation of quadrupolar order, different sets of relaxation delays with appropriate repetition times were used because of a large spread in the magnitude of the relaxation times. The pulse sequence was modified using an additional $\pi/4$ pulse to minimize any long-term instabili-

ty of the spectrometer. This pulse was phase cycled to have a net effect of subtracting the equilibrium magnetization (M_0) signal from the JB signal. Signal collection was started about 5 μs after each monitoring $\pi/4$ pulse, and averaged up to 4096 scans at 15.1 MHz and over 128–512 scans at 46 MHz. T_{1Z} and T_{1Q} were derived from a least-squares fit of the sum $S(t)$ and difference $D(t)$ of the component areas of the quadrupolar doublet:

$$S(t) \propto \exp(-t/T_{1Z}) ,$$

$$D(t) \propto \exp(-t/T_{1Q}) .$$

The subtraction of the M_0 signal in the pulse sequence meant that a simple exponential equation could be used for $S(t)$. The experimental uncertainty in the spin-lattice relaxation times was estimated to be $\pm 5\%$ or better. In determining relaxation rates at the carbon positions 3 and 4, a deconvolution routine using 100% Gaussian lines was used to find the areas of the two peaks under the overlapping peaks, 3 and 4, in Fig. 1(b). The quadrupolar splittings were determined from deuterium NMR spectra obtained by Fourier transforming the free-induction-decay signal after a $\pi/2$ pulse. These splittings had an experimental error of better than $\pm 1\%$. Now T_{1Z} and T_{1Q} are given for spin I=1 by the standard spin relaxation theory [33]

$$\begin{aligned} T_{1Z}^{-1} &= J_1(\omega_0) + 4J_2(2\omega_0) , \\ T_{1Q}^{-1} &= 3J_1(\omega_0) , \end{aligned} \tag{1}$$

which can be used to separate the two spectral densities of motion $J_1(\omega_0)$ and $J_2(2\omega_0)$ at the Larmor frequency $\omega_0/2\pi$ and twice the Larmor frequency, respectively.

III. THEORY

The molecular mean field theory based on the additive potential method has been well documented in the literature [12,31], while the decoupled model that treats the correlated internal and external motion has been described in detail elsewhere [7,10]. The diamond lattice used to describe the carbon-carbon backbone of an alkyl chain was replaced later [32] by a more realistic geometry ($\angle$C–C–H=107.5°, $\angle$H–C–H=113.6°, $\angle$C–C–C=113.5°) [34]. The dihedral angles for rotation of a C—C bond in the chain are $\phi = 0, \pm 112°$ for the three RISs. These RISs correspond to the trans (t) and the two symmetric gauche ($g^{\pm}$) states. The gauche states have higher internal energy in comparison to that of the trans state by an amount E_{tg}. When the chain contains a g^+g^- or a g^-g^+ linkage, an additional internal energy $E_{g^{\pm}g^{\mp}}$ is added because these linkages bring part of the chain near to itself, the so-called "pentane effect." The E_{tg} values reported for gaseous alkanes lie between 2100 and 3200 J/mol, while the $E_{g^{\pm}g^{\mp}}$ value is about three times larger [14]. In this section, we only give the necessary formulas for quadrupolar splitting and spectral densities of motion, and molecular parameters that are relevant to our hexyloxy chain in 6OCB.

We modeled the experimental data in a self-consistent manner by first fitting the quadrupolar splittings to obtain E_{tg}, $E_{g^{\pm}g^{\mp}}$, $\langle P_2 \rangle$, the nematic order parameter, and interaction parameters in the potential of mean torque (X_a for the cyanobiphenyl core including the C_{ar}—O bond, where the subscript ar stands for aromatic, and X_c for a C—C bond). The molecular core was assumed to have cylindrical symmetry. These derived parameters were then used in subsequent fitting of the spectral densities. Using the minimization routine AMOEBA [35], we fitted the quadrupolar splittings at each chosen temperature by minimizing the sum squared error f,

$$f = \sum_i [S_{CD}^{(i)}(\text{expt}) - S_{CD}^{(i)}(\text{calc})]^2 \tag{2}$$

where $S_{CD}^{(i)}$ is the segmental order parameter of the C_i—D bond. The spectral density data at both frequencies was then fitted by minimizing the sum squared percentage error F,

$$F = \sum_{\omega} \sum_{i} \sum_{m_L} \left[\frac{J_{m_L}^{(i)}(m_L\omega)_{\text{expt}} - J_{m_L}^{(i)}(m_L\omega)_{\text{calc}}}{J_{m_L}^{(i)}(m_L\omega)_{\text{expt}}} \times 100 \right]^2 . \tag{3}$$

The sum over i in f included only the S_{CD} data from the methylene deuterons, while in F this sum included the data from the ring and the methylene data from the hexyl chain, i.e., data from the methyl deuterons were not included in either minimization [35]. The fitting quality factor Q in the spectral density calculations is given by the percentage mean-squared deviation

$$Q = \frac{\sum_{\omega} \sum_{i} \sum_{m_L} [J_{m_L}^{(i)}(m_L\omega)_{\text{expt}} - J_{m_L}^{(i)}(m_L\omega)_{\text{calc}}]^2}{\sum_{\omega} \sum_{i} \sum_{m_L} [J_{m_L}^{(i)}(m_L\omega)_{\text{expt}}]^2} \times 100 . \tag{4}$$

The C_{ar}—O bond was taken to be along the biphenyl para axis, as this had speeded up [36] the computation time needed to minimize F. The quadrupolar coupling constant ($q_{CD}^{(i)}$) is taken as 168 and 185 kHz for the methylene and ring deuterons, respectively. We found that in order to give $S_{CD}^{(3)}$ smaller than $S_{CD}^{(4)}$ [29], the $\angle$C–O–C must be between 113° and 120°. The best value could be determined when best fits to both the splitting and spectral density data were obtained over the entire temperature. We assumed the bond interaction parameter of the O—C bond to be the same as X_c of a C—C bond, although their bond lengths were different. The rotational minima about the O—C_{ar} bond of the 6OCB chain were also taken to be 112° [28]. The dihedral angle ϕ_0 formed between the phenyl ring and the plane of the C_{ar}—O and O—C bonds must be treated differently because of higher E_{tg}(COCC) and $E_{g^{\pm}g^{\mp}}$(COCCC). We found that in fitting spectral density data, the O—C bond should take four equivalent sites [8], symmetrically placed with respect to the phenyl ring and the plane perpendicular to it, i.e., $\mp\phi_0$, $\pm(180°-\phi_0)$. We needed to consider either $\mp\phi_0$ or $\pm(180°-\phi_0)$ due to the O—C bond being symmetric with respect to the plane perpendicular to the adjacent phenyl ring. Hence the total num-

ber (N) of conformations of the hexyloxy chain is 486.

In modeling the quadrupolar splittings ($\Delta\nu_i$) of the C_i deuterons, the segmental order parameters are calculated by

$$S_{CD}^{(i)}=2\Delta\nu_i/3q_{CD}^{(i)} \ . \tag{5}$$

Suppose that $S_{\alpha\beta}^{n}$ represents an order parameter tensor that describes the orientational order of the nth rigid conformer. To predict $S_{CD}^{(i)}$ for different methylene deuterons, we note that it is simply a weighted average of the segmental order parameters of all conformations,

$$S_{CD}^{(i)}=\sum_{n=1}^{N} p_{eq}(n)S_{CD}^{n,i} \ , \tag{6}$$

where $p_{eq}(n)$ is the fraction of molecules in the nth conformation. To evaluate $p_{eq}(n)$, we need both the external potential energy $U_{ext}(n,\omega)$ and internal energy $U_{int}(n)$ [12] of the nth conformer. The external potential energy depends also on the orientation ω of the director in a molecular frame, while the internal energy is assumed to depend on the number (N_g) of gauche linkages and the number ($N_{g^{\pm}g^{\mp}}$) of $g^{\pm}g^{\mp}$ linkages in the hexyloxy chain of the nth conformer

$$U_{int}(n)=N_gE_{tg}+N_{g^{\pm}g^{\mp}}E_{g^{\pm}g^{\mp}} \ . \tag{7}$$

We set $E_{tg}(CCCC)=E_{tg}(OCCC)=2150$ J/mol and $E_{g^{\pm}g^{\mp}}(CCCCC)=E_{g^{\pm}g^{\mp}}(OCCCC)=6500$ J/mol [14], but larger values of $E_{tg}(COCC)$ and $E_{g^{\pm}g^{\mp}}(COCCC)$ were tested.

To calculate the spectral densities for a methylene deuteron, one needs to solve a master rate equation to obtain the conditional probability $p_{il_0}(t)$, which gives the probability that the chain assumes configuration i at time t when at time $t=0$ the chain is in configuration l. The transition rate matrix $\tilde{R}$ contains model parameters of internal chain dynamics, i.e., k_1, k_2, and k_3. After symmetrizing this $\tilde{R}$ matrix and then diagonalizing to obtain N eigenvalues Λ_n (real and negative) and eigenvectors $\mathbf{x}^n$, $p_{il_0}(t)$ is given by

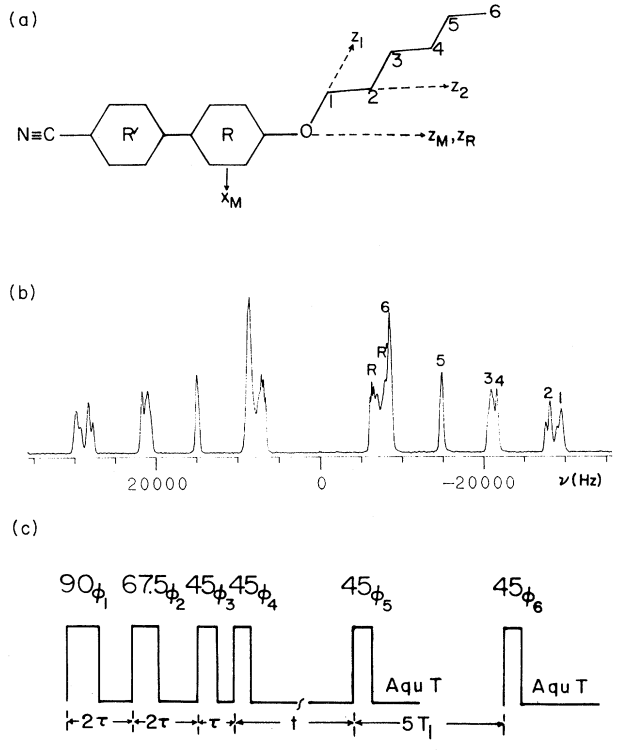

FIG. 1. (a) Schematic diagram of a 6OCB molecule and various coordinate systems used. (b) A typical deuteron NMR spectrum of 6OCB-d_{21}. (c) Modified broadband Jeener-Broekaert sequence.

$$p_{il_0}(t)=x_i^{(1)}(x_l^{(1)})^{-1}\sum_{n=1}^{N} x_i^{(n)}x_l^{(n)}\exp(-|\Lambda_n|t) \ . \tag{8}$$

In the decoupled model, the spectral densities $J_{m_L}^{(i)}(m_L\omega)$ for $m_L\neq 0$ of the C_i deuterons are found by Fourier transforming the correlation functions to give

$$J_{m_L}^{(i)}(m_L\omega)=\frac{3\pi^2}{2}(q_{CD}^{(i)})^2\sum_{m_M}\sum_{n=1}^{N} c_{m_Lm_M}\left|\sum_{l=1}^{N} d_{m_M0}^{2}(\beta_{M,Q}^{(i)l})\exp[-im_M(\alpha_{M,Q}^{(i)l})]x_l^{(1)}x_l^{(n)}\right|^2 \times\sum_j a_{m_Lm_M}^{(j)}\frac{[(\tau_{m_Lm_M}^{(j)})^{-1}+|\Lambda_n|]}{\{(m_L\omega)^2+[(\tau_{m_Lm_M}^{(j)})^{-1}+|\Lambda_n|]^2\}} \ , \tag{9}$$

where $\beta_{M,Q}^{(i)l}$ and $\alpha_{M,Q}^{(i)l}$, the polar angles of the C_i—D bond of the lth conformed in the M frame [see Fig. 1(a)], $a_{m_Lm_M}^{(j)}$, and $b_{m_Lm_M}^{(j)}$ represent, respectively, normalized relative weights and decay time constants in multiexponentials of the correlation functions, and $c_{m_Lm_M}$ are the mean squares of the Wigner rotation matrices. The rotational correlation times $\tau_{m_Lm_M}^{(j)}$ are given in Nordio's model by

$$\tau_{m_Lm_M}^{(j)}=b_{m_Lm_M}^{(j)}/[6D_\perp+m_M^2(D_\parallel-D_\perp)] \ , \tag{10}$$

where $D_\parallel$ and $D_\perp$ are the rotational diffusion constants of an "average" conformer about its long Z_M axis and of this axis. The a, b, and c coefficients depend on the order parameter $\langle P_2\rangle$ and are tabulated [17] for a Maier-Saupe potential. The spectral densities for the ring deuterons are given by the model of superimposed rotations [2,31],

$$J^{(R)}_{m_L}(m_L\omega)=\frac{3\pi^2}{2}(q^{(R)}_{\mathrm{CD}})^2\sum_{m_M m_R}\sum c_{m_L m_M}[d^2_{m_R 0}(\beta_{R,Q})]^2[d^2_{m_M m_R}(\beta_{M,R})]^2$$
$$\times\sum_j a^{(j)}_{m_L m_M}\frac{[(\tau^{(j)}_{m_L m_M})^{-1}+(1-\delta_{m_R 0})D_R]}{\{(m_L\omega)^2+[(\tau^{(j)}_{m_L m_M})^{-1}+(1-\delta_{m_R 0})D_R]^2\}}\ , \tag{11}$$

where $\beta_{M,R}$, the angle between the para axis and the Z_M axis, is zero, $\beta_{R,Q}$, the angle between the ring C—D bond and the para axis, is 60°, and the internal ring rotation about its para axis is assumed to be free in the strong collision limit and is described by a diffusion constant D_R. The next section describes results of minimizations of errors in fits of experimental splitting and spectral density data.

IV. RESULTS AND DISCUSSION

A. Orientational ordering

The experimental segmental order parameters $S^{(i)}_{\mathrm{CD}}$ are plotted as a function of temperature in Fig. 2. Equation (6) is used in our mean field calculations of the segmental order parameter profiles at different temperatures. Since $S^{(3)}_{\mathrm{CD}} < S^{(4)}_{\mathrm{CD}}$, a ∠C–O–C of 119° was found to give best fits of the splitting and spectral density data. In a number of aromatic compounds, the ∠C–O–C was found to vary between 115° and 125° depending on the compound. Hence our ∠C–O–C appears to be very reasonable. Since the segmental order parameters were independent of the dihedral angle ϕ_0, its value could only be determined by fitting the spectral density data. The final value of 70° was established by fitting the spectral density data over the entire temperature range. Despite the fact that we separately minimized the functions f and F, both the geometry and internal energies involving the oxygen atom were determined through iterative fitting of the static and dynamic NMR observables in 6OCB. We used the accepted RIS gauche energies [E_{tg}(CCCC)=2150 J/mol, $E_{g\pm g\mp}$ (CCCCC) =6500 J/mol]. This $E_{g\pm g\mp}$ value is comparable to that used in fitting quadrupolar splittings of MBBA [32]. The "best" internal energy values found for E_{tg} (COCC) and $E_{g\pm g\mp}$ (COCCC) were 3300 J/mol and 12 kJ/mol, respectively. Thus E_{tg}

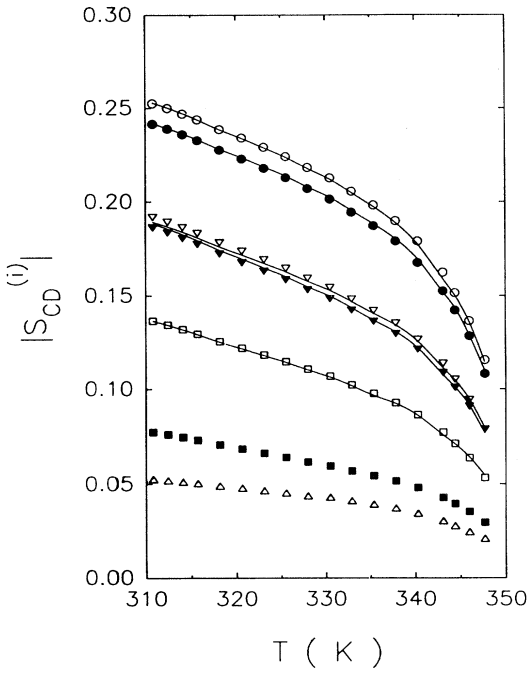

FIG. 2. Plots of segmental order parameters as a function of temperature in the nematic phase of 6OCB-d_{21}. ○, ▽, and □ represent C_1, C_4, and C_5, while the corresponding solid symbols represent C_2, C_3, and C_6. △ represents C_0, where the subscript 0 represents the ring R. The solid curves denote the theoretical predictions of the molecular mean field theory.

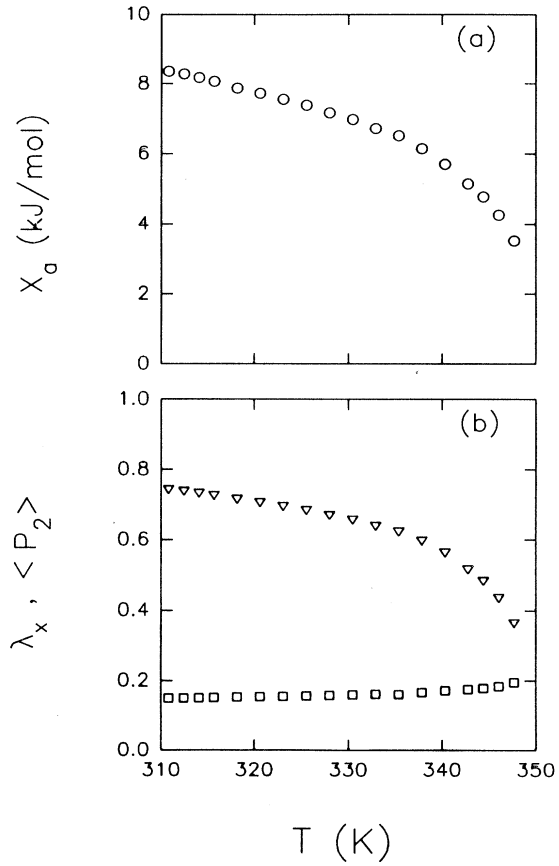

FIG. 3. Plots of derived interaction parameters X_a (a) and λ_x, as well as the nematic order parameter $\langle P_2 \rangle$ (b) of 6OCB as a function of temperature.

TABLE I. Interaction parameters and order parameters of the average conformer derived from optimization of fits to experimental quadrupolar splittings of 6OCB.

T (K)	X_a (kJ/mol)	X_c (kJ/mol)	$\langle P_2 \rangle$	$\langle S_{xx} \rangle$-$\langle S_{yy} \rangle$	$10^5 f$
310.8	8.352	1.256	0.741	0.0189	1.1
314.1	8.175	1.239	0.731	0.0194	1.0
318.2	7.872	1.208	0.714	0.0202	0.9
323.1	7.552	1.175	0.694	0.0211	0.8
328.0	7.164	1.138	0.669	0.0223	0.7
335.4	6.510	1.054	0.622	0.0239	1.0
340.3	5.701	0.984	0.562	0.0266	0.8
344.4	4.774	0.854	0.483	0.0281	0.4
347.7	3.530	0.689	0.363	0.0292	1.1

(COCC) is about 1.5 times E_{tg} (CCCC). The upper limit of $E_{g^{\pm}g^{\mp}}$ (COCCC) seemed to be insensitive in minimizing the f or F value. However, the fits to S_{CD} at the carbon positions 1 and 2 were significantly improved by making $E_{g^{\pm}g^{\mp}}$ (COCCC) larger than $E_{g^{\pm}g^{\mp}}$ (CCCCC). By fixing the molecular geometry and all gauche energies, a two-parameter (X_a, X_c) fit was carried out at each chosen temperature, resulting in f of the order of 10^{-5} (see Table I) over the entire nematic range. The predictions of the methylene segmental order parameters by the additive potential method are also shown in Fig. 2. The derived interaction parameters X_a and $\lambda_x (= X_c / X_a)$, and the nematic order parameter $\langle P_2 \rangle$ are plotted in Fig. 3 as a function of temperature. The $\langle P_2 \rangle$ of an average conformer was obtained by calculating the conformationally averaged order matrix $\langle S \rangle$ from $p_{eq}(n)$ and $S^n_{\alpha\beta}$. By diagonalizing $\langle \mathbf{S} \rangle$, its principal components are $\langle P_2 \rangle$ and $\langle S_{xx} \rangle$-$\langle S_{yy} \rangle$. Since the magnitude of $\langle S_{xx} \rangle$-$\langle S_{yy} \rangle$ is small (see Table I), the average conformer is essentially a cylinder and its long z axis is very close to the ring para axis. Thus the ring para axis will be used to define the long diffusion axis of 6OCB when overall rotation is examined. In Table I, we list some interaction parameters, orientational order parameters, and f. These interaction parameters and $\langle P_2 \rangle$ are used below to model the spectral density data.

B. Molecular and internal rotations

An earlier attempt to interpret the spectral density data of 6OCB [26] with the decoupled model met with limited success. As mentioned above, we have remeasured these at 15.1 and 46 MHz with a better signal to noise ratio. These are plotted as a function of temperature in Fig. 4. They agree well with those reported be-

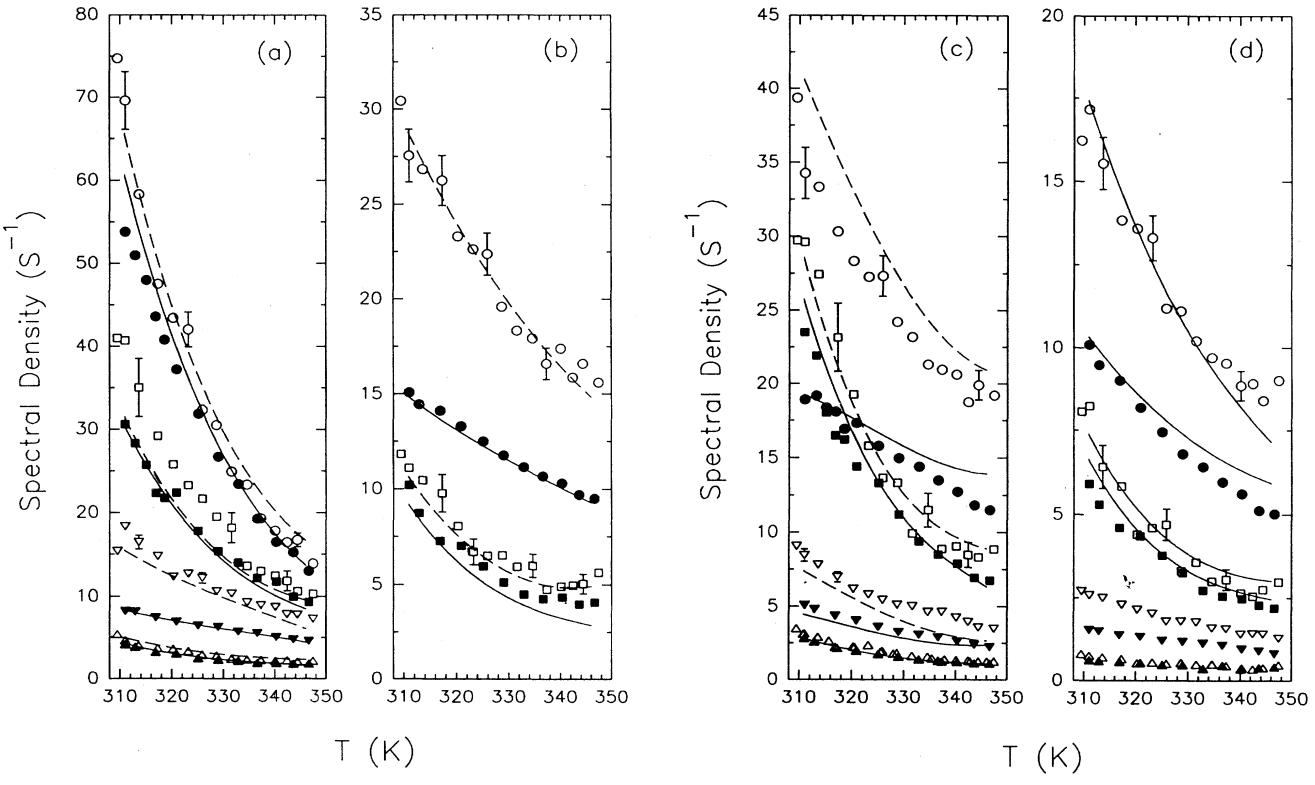

FIG. 4. Plots of spectral densities vs temperature in 6OCB-d_{21}. Open symbols denote 15.1 MHz data, while solid symbols denote 46 MHz data. (a) ○ and □ denote $J_1^{(R)}(\omega)$ and $J_2^{(R)}(2\omega)$, while ▽ and △ denote $J_1^{(4)}(\omega)$ and $J_2^{(4)}(2\omega)$, respectively; (b) ○ and □ denote $J_1^{(2)}(\omega)$ and $J_2^{(2)}(2\omega)$. (c) ○ and □ denote $J_1^{(1)}(\omega)$ and $J_1^{(1)}(2\omega)$, while ▽ and △ denote $J_1^{(5)}(\omega)$ and $J_2^{(5)}(2\omega)$, respectively; (d) ○ and □ denote $J_1^{(3)}(\omega)$ and $J_2^{(3)}(2\omega)$, while ▽ and △ denote $J_1^{(6)}(\omega)$ and $J_2^{(6)}(2\omega)$, respectively. Solid and dashed curves are theoretical predictions based on Nordio's model and the decoupled model for 15.1 and 46 MHz, respectively.

TABLE II. Jump rate constants (in units of 10^9 s^{-1}) for 6OCB derived using the decoupled model and Nordio's model of rotational diffusion.

T (K)	k_1	k_2	k_3	F	Q (%)
311	2.1×10^3	7.6×10^2	1.7×10^5	1.6×10^3	1.2
316	2.1×10^3	9.3×10^2	4.0×10^5	1.4×10^3	1.1
321	2.0×10^3	1.3×10^3	2.4×10^6	1.5×10^3	1.1
328	1.7×10^3	2.1×10^3	7.4×10^6	1.6×10^3	1.1
335	1.3×10^3	3.5×10^3	9.6×10^7	2.4×10^3	1.3
338	1.1×10^3	4.7×10^3	2.2×10^7	2.9×10^3	1.3
343	6.3×10^2	9.0×10^3	1.3×10^9	3.6×10^3	1.5

fore, except that minor differences exist at carbon position 1 and at ring R. As before, the spectral densities of the cyano ring (R') have not been measured because of a severe overlap with the methyl signal. The spectral densities of the methylene and ring deuterons are calculated using Eqs. (9) and (11), respectively. These involve the following model parameters: rotational diffusion constants $D_\parallel$ and $D_\perp$ for molecular rotation, and D_R for internal ring rotation, as well as three jump rates k_1, k_2, and k_3 for the internal bond motions. There are a total of twelve $J_1(\omega)$ (six per frequency) and twelve $J_2(2\omega)$ at each chosen temperature, from which six model parameters are varied to achieve a minimum F. As seen in Table II, F varies between 1400 and 3600. These compare with the F value of 1500 estimated based on the experimental uncertainties. Although the F values increase significantly near the clearing temperature, the corresponding Q's (Table II) compare favorably with those reported for MBBA [32] and 5CB [10,36]. The predicted spectral densities of the ring and the carbon positions 1–5 at both Larmor frequencies as a function of temperature are also shown in Fig. 4 for direct comparison with the experiment. We note that the agreement between theory and experiment was generally very good. Those deviations that did occur are mostly within the bounds of error as indicated by the experimental error bars. The experimental and predicted site dependences of the spectral densities are shown in Fig. 5 for 316 and 335 K. On close examination of Figs. 4 and 5, the model underestimates several spectral densities $J_1^{(4)}(\omega)$, $J_1^{(5)}(\omega)$, and $J_2^{(R)}(2\omega)$, and overestimates $J_1^{(1)}(\omega)$, as well as $J_1^{(3)}(\omega)$ to some extent.

The temperature dependences of the three rotational diffusion constants are plotted in Fig. 6. As seen in this figure, $D_\perp$, $D_\parallel$, and D_R all show Arrhenius relationships with temperature; the corresponding activation energies (E_a) are 21±24, 39±20, and 34±25 kJ mol^{-1}, respectively. The E_a value for the tumbling motion ($D_\perp$) is small (and has a much larger uncertainty) compared with the value for the spinning motion ($D_\parallel$), which is of course unphysical. This merely reflects the difficulty in getting information about tumbling motion of the molecule as in previous studies [6,10,32]. Over the temperature range

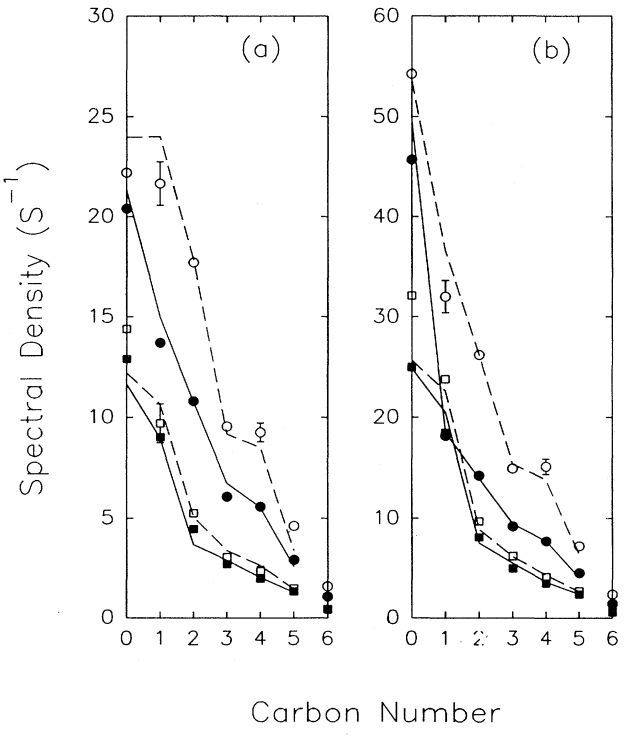

FIG. 5. Plot of the densities $J_1(\omega)$ (○) and $J_2(2\omega)$ (□) at (a) 335 K and (b) 316 K. Open symbols denote 15.1 MHz data, while solid symbols denote 46 MHz data. Solid and dashed lines are theoretical predictions at 15.1 and 46 MHz from Nordio's model and the decoupled model.

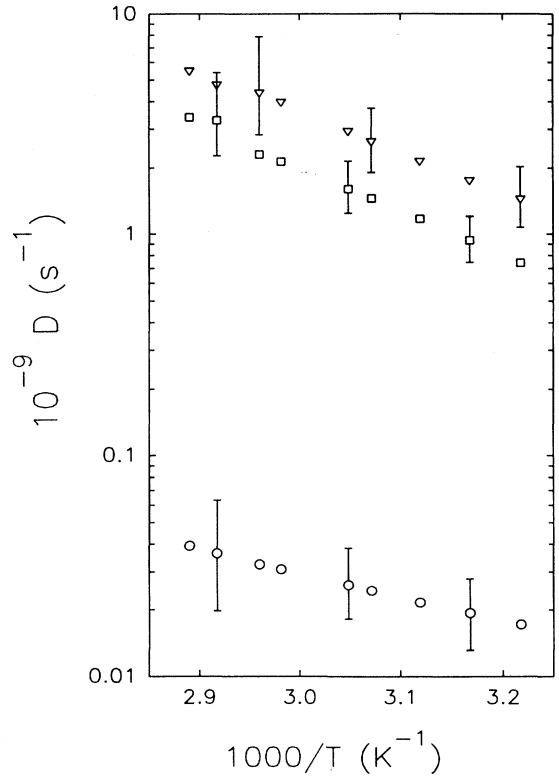

FIG. 6. Plots of rotational diffusion constants D_R (▽), $D_\parallel$ (□), and $D_\perp$ (○) vs the reciprocal temperature in 6OCB.

studied $D_{\parallel}$ is approximately $60D_{\perp}$, and $D_R/D_{\parallel} \simeq 2$. We used the table of a,b,c coefficients [17] which is applicable for $D_{\parallel}=D_{\perp}$ only. This is an approximation, since our $D_{\parallel} \simeq 60D_{\perp}$. The approximation is acceptable as long as internal rotations are fast. The error bars shown in Fig. 6 were estimated by changing the parameter in question to double the F value while keeping all the remaining parameters fixed at those found in the minimization. The derived jump rates are summarized in Table II. Both k_2 and k_3 increase with temperature, thereby showing thermally activated two- and three-bond motions in the hexyl chain. The magnitudes of k_1 and k_2 are roughly the same, but k_1 decreases gradually with increasing temperature. This temperature behavior of k_1 is also observed in 5CB [36]. It is noted that k_3 describes the so-called kink motion in the chain. It appears to be rather large, especially as the clearing point is approached. This has to do with a large upper error bound for this rate constant and is probably linked to the assumption of four equivalent sites for the O—C bond. It would be of interest to see if MD calculations could also monitor the rates of these internal motions.

V. SUMMARY AND CONCLUSION

We have successfully modeled both static and dynamic NMR observables in a perdeuterated 6OCB sample. The assignment [29] of quadrupolar splittings in deuterated 6OCB is further supported by our deuteron relaxation data. It should be emphasized that modeling the splittings alone could not provide a critical test of the molecular mean field theory, especially when there were uncertainties in molecular geometry and gauche energies. Hence, simultaneous fits of both splitting and spectral density data appear to be desirable. The values of E_{tg} and $E_{g^{\pm}g^{\mp}}$ used here for 6OCB are not forced high (3500–3800 J/mol for E_{tg} [12,25,26,34]) in order to explain the segmental order profile. This was one of the main objections to the simple additive potential method of Emsley, Luckhurst, and Stockley [12]. The decoupled model provides a simple description of correlated internal bond rotations in the chain. The overall motion of an average conformer is parametrized by two rotational diffusion constants, one for the spinning motion ($D_{\parallel}$) and the other for the tumbling motion ($D_{\perp}$). The activation energy of the tumbling motion is again not well defined by looking even at different sites of a perdeuterated 6OCB molecule. It is noted here that these rotational diffusion constants and their ratios ($D_{\parallel}/D_{\perp}$) could be slightly modified if director fluctuations made a small but nonzero contribution to the spectral densities J_1's. The present work shows that conformations of an alkyloxy chain must be generated differently than those of an alkyl chain, e.g., in 5CB and MBBA. We note that k_1 only affects the spectral densities of deuterons at the penultimate carbon and the methyl groups. Since the methyl group has not been included in the minimization because of its unusual dynamics [8], the determination of k_1 for one-bond motion may be hampered. In conclusion, despite many simplifying assumptions used in the decoupled model [7], the quality of fits to the available spectral densities is more than satisfactory over the entire nematic range. As the chain length increases, the computation efforts become more demanding, but the motional model can be more stringently tested. We hope that MD calculations with realistic atom-atom potentials can further complement NMR studies of liquid crystals. The present study further supports the usefulness of the decoupled model in describing correlated internal chain dynamics in liquid crystals.

ACKNOWLEDGMENT

The financial support of the Natural Science and Engineering Council of Canada and Brandon University are gratefully acknowledged. We thank N. Finlay for his technical support and C. Price for his assistance in computer programming.

[1] See, for example, R. Y. Dong, J. Lewis, E. Tomchuck, and E. Bock, J. Chem. Phys. **69**, 5314 (1978); H. Hutton, E. Bock, E. Tomchuck, and R. Y. Dong, *ibid.* **68**, 940 (1978).
[2] P. A. Beckmann, J. W. Emsley, G. R. Luckhurst, and D. L. Turner, Mol. Phys. **50**, 699 (1983); **59**, 97 (1986); C. R. J. Counsell, J. W. Emsley, G. R. Luckhurst, D. L.Turner, and J. Charvolin, *ibid.* **52**, 499 (1984).
[3] R. Y. Dong and K. R. Sridharan, J. Chem. Phys. **82**, 4838 (1985); R. Y. Dong, J. Magn. Res. **66**, 422 (1986); J. Chem. Phys. **88**, 3962 (1988).
[4] T. M. Barbara, R. R. Vold, and R. L. Vold, J. Chem. Phys. **79**, 6338 (1983); T. M. Barbara, R. R. Vold, R. L. Vold, and M. E. Neubert, J. Chem. Phys. **82**, 1612 (1985).
[5] D. Goldfarb, R. Y. Dong, Z. Luz, and H. Zimmerman, Mol. Phys. **54**, 1185 (1985).
[6] J. M. Goetz, G. L. Hoatson, and R. L. Vold, J. Chem. Phys. **97**, 1306 (1992).
[7] R. Y. Dong and G. M. Richards, Chem. Phys. Lett. **171**, 389 (1990); R. Y. Dong, Phys. Rev. A **43**, 4310 (1991).
[8] A. Ferrarini, G. J. Moro, and P. L. Nordio, Liq. Cryst. **8**, 593 (1990).
[9] R. Y. Dong and G. M. Richards, Chem. Phys. Lett. **200**, 54 (1992).
[10] R. Y. Dong and G. M. Richards, J. Chem. Soc. Faraday Trans. **88**, 1885 (1992).
[11] R. Köllner, K. H. Schweikert, and F. Noack, Liq. Cryst. **13**, 483 (1993).
[12] J. W. Emsley, G. R. Luckhurst, and C. P. Stockley, Proc. R. Soc. London, Ser. A **381**, 117 (1982).
[13] E. T. Samulski and R. Y. Dong, J. Chem. Phys. **77**, 5090 (1982).
[14] P. J. Flory, *Statistical Mechanics of Chain Molecules* (Interscience, New York, 1969).
[15] R. J. Wittebort and A. Szabo, J. Chem. Phys. **69**, 1722 (1978).
[16] P. L. Nordio and P. Busolin, J. Chem. Phys. **55**, 5485 (1971); P. L. Nordio, G. Rigatti, and U. Segre, *ibid.* **56**, 2117 (1972); Mol. Phys. **25**, 129 (1973).

[17] R. R. Vold and R. L. Vold, J. Chem. Phys. **88**, 1443 (1988).
[18] C. F. Polnaszek, G. V. Bruno, and J. H. Freed, J. Chem. Phys. **58**, 3185 (1973); C. F. Polnaszek and J. H. Freed, *ibid*. **79**, 2283 (1975).
[19] M. P. Allen and M. R. Wilson, J. Comp. Aid. Mol. Des. **3**, 335 (1989).
[20] S. J. Picken, W. F. van Gunsteren, P. T. van Duijnen, and W. H.De Jeu, Liq. Cryst. **6**, 357 (1989).
[21] A. V. Komolkin, A. Laaksonen, and A. Maliniak, J. Chem. Phys. **101**, 4103 (1994).
[22] C. W. Cross and B. M. Fung, J. Chem. Phys. **101**, 6839 (1994).
[23] I. Ono and S. Kondo, Mol. Cryst. Liq. Cryst. Lett. **8**, 69 (1991).
[24] M. R. Wilson and M. P. Allen, Mol. Cryst. Liq. Cryst. **198**, 465 (1991); Liq. Cryst. **12**, 157 (1992); S. Ye. Yakovenko, A. A. Minko, G. Krömer, and A. Geiger, Liq. Cryst. **17**, 127 (1994).
[25] C. J. R. Counsell, J. W. Emsley, G. R. Luckhurst, and H. S. Sachdev, Mol. Phys **63**, 33 (1988).
[26] R. Y. Dong and G. Ravindranath, Liq. Cryst. **17**, 47 (1994); R. Y. Dong and G. W. O'Bannon, Mol. Cryst. Liq. Cryst. **209**, 139 (1991).
[27] C. D. Poon, C. M. Wooldridge, and B. M. Fung, Mol. Cryst. Liq. Cryst. **157**, 303 (1988).
[28] D. J. Photinos, E. T. Samulski, and H. Toriumi, J. Chem. Phys. **94**, 2758 (1991).
[29] J. W. Emsley, E. K. Foord, P. J. F. Gandy, D. L. Turner, and H. Zimmermann, Liq. Cryst. **17**, 303 (1994).
[30] P. Pincus, Solid State Commun. **7**, 415 (1969).
[31] R. Y. Dong, *Nuclear Magnetic Resonance of Liquid Crystals* (Springer-Verlag, New York, 1994).
[32] R. Y. Dong, L. Friesen, and G. M. Richards, Mol. Phys. **81**, 1017 (1994).
[33] J. P. Jacobsen, H. K. Bildsoe, and K. Schumberg, J. Magn. Res. **23**, 153 (1976); S. B. Ahmad, K. J. Packer, and J. M. Ramsden, Mold. Phys. **33**, 857 (1977); R. R. Vold and R. L. Vold, J. Chem. Phys. **66**, 4018 (1977).
[34] C. J. R. Counsell, J. W. Emsley, N. J. Heaton, and G. R. Luckhurst, Mol. Phys. **54**, 847 (1985).
[35] W. H. Press, B. P. Flannery, S. A. Tenkolsky, and W. T. Vetterling, *Numerical Recipes* (Cambridge University, Cambridge, England, 1986).
[36] R. Y. Dong and G. M. Richards, Mol. Cryst. Liq. Cryst. (to be published).